Asymptotic normalization coefficients for $^{13}C+p\rightarrow{}^{14}N$

L. Trache, A. Azhari, H. L. Clark, C. A. Gagliardi, Y.-W. Lui, A. M. Mukhamedzhanov, and R. E. Tribble
Cyclotron Institute, Texas A&M University, College Station, Texas 88743-3366

F. Carstoiu
Institute of Physics and Nuclear Engineering, Bucharest, Romania

(Received 12 June 1998)

The $^{13}C(^{14}N,^{13}C)^{14}N$ proton exchange reaction has been measured at an incident energy of 162 MeV. Angular distributions were obtained for proton transfer to the ground and low-lying excited states in ^{14}N. Elastic scattering of ^{14}N on ^{13}C also was measured out to the rainbow angle region in order to find reliable optical model potentials. Asymptotic normalization coefficients for the system $^{13}C+p\rightarrow{}^{14}N$ have been found for the ground state and the excited states at 2.313, 3.948, 5.106, and 5.834 MeV in ^{14}N. These asymptotic normalization coefficients will be used in a determination of the *S* factor for $^{7}Be(p,\gamma)^{8}B$ at solar energies from a measurement of the proton transfer reaction $^{14}N(^{7}Be,^{8}B)^{13}C$. [S0556-2813(98)03111-2]

PACS number(s): 25.70.Hi, 25.70.Bc, 21.10.−k, 24.10.Eq

I. INTRODUCTION

The asymptotic normalization coefficient C for the system $A+p\leftrightarrow B$ specifies the amplitude of the single-proton tail of the wave function for nucleus B when the core A and the proton are separated by a distance large compared to the strong interaction radius. In previous reports [1,2], we have shown that knowledge of asymptotic normalization coefficients (ANC's) can be used to calculate the direct capture rates for (p,γ) or (α,γ) reactions of astrophysical interest when the captured p or α is relatively loosely bound in the final nucleus. The required ANC's can often be measured in peripheral transfer reactions. We are using the ANC technique to determine the astrophysical S factor $S_{17}(0)$ for the proton radiative capture reaction $^{7}Be(p,\gamma)^{8}B$ at solar energies, using the transfer reactions $^{10}B(^{7}Be,^{8}B)^{9}Be$ and $^{14}N(^{7}Be,^{8}B)^{13}C$. In order to extract the ANC for $^{7}Be+p\rightarrow{}^{8}B$ from these measurements, we must know the ANC's for the $^{9}Be+p\rightarrow{}^{10}B$ and $^{13}C+p\rightarrow{}^{14}N$ systems. We report below a study of $^{14}N+{}^{13}C$ elastic scattering and the proton exchange reaction $^{13}C(^{14}N,^{13}C)^{14}N$ at 162 MeV, from which we find the ANC's corresponding to $^{13}C+p\rightarrow{}^{14}N$. The experiment is similar to our measurement of the $^{9}Be+p\rightarrow{}^{10}B$ ANC's reported earlier [3].

Below we present details of the experiment. This is followed by a discussion of the optical model parameters extracted from the elastic scattering data and then the results for the ANC's found from the proton exchange reaction.

II. THE EXPERIMENT

The experiment was performed using a ^{14}N beam from the Texas A&M University K500 superconducting cyclotron and the Multipole Dipole Multipole magnetic spectrometer [4]. A 300 $\mu g/cm^2$ self-supporting target of 99% enriched ^{13}C was bombarded with a well collimated 162 MeV $^{14}N^{+3}$ beam. The angular spread of the beam on target was less than $\Delta\theta=0.1°$ after passing through the beam analysis system [5]. Both elastic scattering and the proton transfer reaction were measured during the same run. The elastic scattering data were used to assess the possible effects of interference between the elastic scattering and exchange processes and to extract optical model parameters for use in the distorted-wave Born approximation (DWBA) calculations of the proton exchange reaction. The elastic scattering results were also used in the normalization of the cross sections for the transfer reaction. The experimental setup was identical to that used in the $^{10}B+{}^{9}Be$ experiment and was described in detail in Ref. [3]. For the present experiment, the spectrometer's entrance aperture was set at $\Delta\theta=4°$ (horizontal) and $\Delta\varphi=1°$ (vertical). The modified Oxford detector [6] was used in the focal plane. The detector consists of a 50 cm long gas ionization chamber to measure the specific energy loss of particles in the gas and their focal plane position at four resistive wires, separated by 16 cm along the particles' trajectories, followed by an NE102A plastic scintillator to measure the residual energy. The entrance and exit windows of the detector were made of 1.8 and 7.2 mg/cm^2 thick Kapton foils, respectively. The ionization chamber was filled with purified isobutane at a pressure of 30 Torr.

Elastic scattering data were obtained over the laboratory angular range $\theta_{lab}=2°-34°$, corresponding to the center-of-mass range $\theta_{c.m.}=4°-70°$, by detecting $^{14}N^{+7}$ in the focal plane of the spectrometer. The proton exchange reaction was measured by retuning the magnetic fields of the spectrometer for the rigidity of the outgoing $^{13}C^{+6}$ in the forward angle range $\theta_{lab}=-3°$ to $+18°$. This is kinematically equivalent to measuring elastic or inelastic scattering at the complementary backward angles. Particle identification was accomplished by using the energy loss measured in the ionization chamber and the residual energy as determined by the light output from the plastic scintillator. The focal plane position and the scattering angle at the target were reconstructed using the position measurements from any two of the four wires in the detector, coupled with RAYTRACE [7] calculations. Typically we used the position at the first wire in the detector and that at the wire closest to the focal plane. The spectrometer angular acceptance range of 4 ° was divided into eight bins of 0.5° each during the data analysis. As a check on the reconstruction, we calibrated the target scatter-

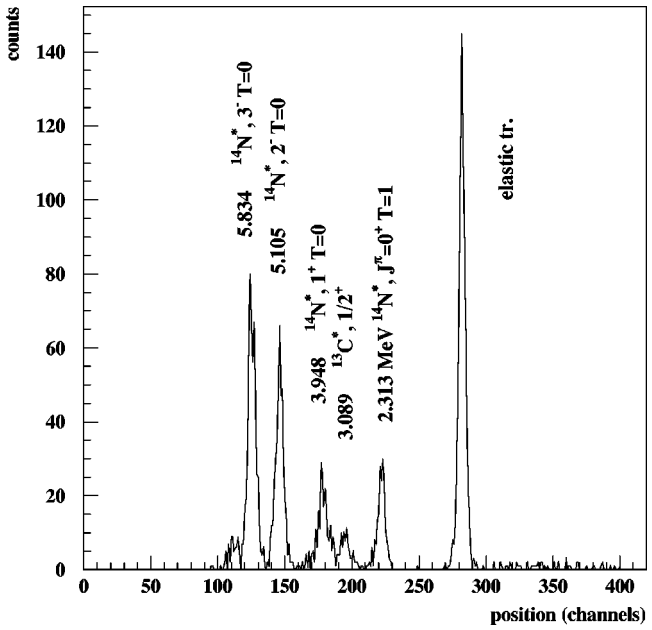

FIG. 1. Spectrum of the proton exchange reaction ^{13}C(^{14}N,^{13}C)^{14}N measured at $\theta_{\rm lab}=8°$.

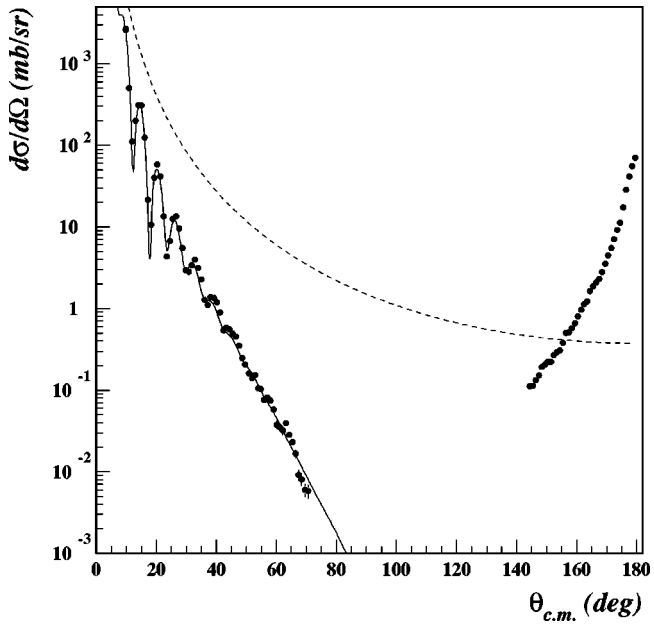

FIG. 2. The angular distribution for elastic scattering of ^{14}N on ^{13}C. The data in the forward hemisphere were obtained by measuring the elastically scattered $^{14}N^{+7}$, while those in the backward hemisphere were obtained by measuring the transfer reaction product $^{13}C^{+6}$ at the complementary forward angles. The dashed curve shows the Rutherford scattering cross section, and the solid curve shows the cross section calculation with potential P1 of Table I.

ing angle determination using an angle mask with five slits $\Delta\theta=0.1°$ wide, uniformly distributed across the 4° opening. These measurements also indicated that the total angular resolution for the experiment was $\Delta\theta_{\rm lab}=0.2°$. The low-lying excited states in both ^{13}C and ^{14}N are well known. Thus, the focal plane energy calibration was straightforward. Typically the spectrometer was moved in 3° steps, allowing for an angle overlap between measurements to check for consistency in the results. Due to the high purity of the target, elastic scattering data were obtained down to $\theta_{\rm lab}=2.5°$ without contamination from heavier elements in the target. By combining measurements of the target thickness with the normalization to elastic scattering at very forward angles, the absolute cross sections for the proton transfer reactions have been determined with an uncertainty of 7%. A spectrum for the proton transfer reaction taken at $\theta_{\rm lab}=8°$ is shown in Fig. 1. In addition to transfer between the ground states of ^{14}N and ^{13}C (elastic proton exchange), we see transitions populating the first (2.313 MeV,$J^\pi=0^+,T=1$), second (3.948 MeV,$J^\pi=1^+,T=0$), fourth (5.106 MeV,$J^\pi=2^-,T=0$), and sixth (5.834 MeV,$J^\pi=3^-,T=0$) excited states of ^{14}N and the first excited state of ^{13}C(3.089 MeV,$J^\pi=1/2^+$), where excitation energies, spins, and parities have been taken from Ref. [8].

III. OPTICAL MODEL POTENTIALS

The measured elastic scattering angular distribution is shown in Fig. 2. Data at forward angles are from normal kinematics elastic scattering, while the data at back angles have been taken from the ^{13}C(^{14}N,^{13}C)^{14}N reaction at forward angles, populating the ground states of both ^{13}C and ^{14}N. While the forward angle data involving proton exchange are kinematically equivalent to elastic scattering at back angles, it is clear from the figure that potential scattering and the proton transfer mechanism completely dominate at forward and backward angles, respectively. We thus treat the data in the two angular ranges independently and do not consider any interference between the amplitudes of the two processes.

The forward angle data have been fit using the code OPTIMIX [9] in a standard optical model analysis using Woods-Saxon volume form-factors for the potential

$$U(r)=-[Vf_V(r)+iWf_W(r)], \tag{1}$$

with the usual notation where

$$f_x(r)=\left[1+\exp\frac{r-r_x(A_1^{1/3}+A_2^{1/3})}{a_x}\right]^{-1}. \tag{2}$$

V and W are the depths of the real and imaginary potentials, A_1 and A_2 are the nuclear masses, r_x and a_x are the reduced radii and diffuseness of the potentials, and x can be either V or W for the real and imaginary parts of the potentials, respectively. Only the central potential terms have been included since vector and higher rank tensor spin-orbit couplings have negligible impact on the cross sections.

Five distinct families of potentials were found in the chi square analysis of the data. Their parameters are presented in Table I, and the fits are compared with the forward angle data in Fig. 3. Included in the table are the volume integrals per pair of interacting nucleons for the real and imaginary parts of the potentials (J_V and J_W), their rms radii (R_V and R_W), and the total reaction cross section calculated in the Glauber model. We note that the volume integrals increase regularly from one family to the next, indicating that no family was missed during the automatic search for the minima. The five potential sets reproduce the total reaction cross section $\sigma_R=1463(100)$ mb measured by DiGregorio *et al.* at

TABLE I. The parameters of the Woods-Saxon optical model potentials extracted from the analysis of the elastic scattering data for ^{14}N(162 MeV)+^{13}C. $r_C=1$ fm for all potentials.

Pot.	V [MeV]	W [MeV]	r_V [fm]	r_W [fm]	a_V [fm]	a_W [fm]	χ^2	σ_R [mb]	J_V [MeV fm^3]	R_V [fm]	J_W [MeV fm^3]	R_W [fm]
P1	79.22	30.27	0.96	1.05	0.76	0.72	17.4	1542	221	4.52	104	4.69
P2	134.76	35.23	0.88	1.05	0.75	0.67	18.3	1525	299	4.28	120	4.61
P3	176.03	35.84	0.86	1.07	0.72	0.65	23.3	1527	361	4.15	125	4.62
P4	241.36	37.45	0.82	1.06	0.71	0.66	27.5	1533	438	4.00	129	4.61
P5	306.44	39.14	0.81	1.05	0.68	0.68	36.1	1552	522	3.90	132	4.61

161.3 MeV [10]. All of the potentials give reasonable χ^2, but potential P1 listed in the table gives the smallest value and is the only one that fits the data at largest angles. This potential also has a real volume integral per pair of interacting nucleons close to that we found (206 MeV fm^3) for the preferred potential in our previous study of ^{10}B+^{9}Be elastic scattering at similar velocities [3]. Hence, we have adopted potential P1 for the DWBA calculations of the proton transfer process, while the others are used to estimate the uncertainty due to the choice of optical model parameters. Further details concerning the potential model analysis will be discussed in a future publication.

IV. ASYMPTOTIC NORMALIZATION COEFFICIENTS

For a peripheral transfer reaction, ANC's are extracted from the measured angular distribution by comparison to a DWBA calculation. Consider the proton transfer reaction $a+A\rightarrow c+B$, where $a=c+p$ and $B=A+p$. The experimental cross section is related to the DWBA according to

$$\frac{d\sigma}{d\Omega}=\sum_{l_Bj_Bl_aj_a}(C^B_{Apl_Bj_B})^2(C^a_{cpl_aj_a})^2R_{l_Bj_Bl_aj_a}, \tag{3}$$

where

$$R_{l_Bj_Bl_aj_a}=\frac{\tilde{\sigma}^{DW}_{l_Bj_Bl_aj_a}}{b^2_{Apl_Bj_B}b^2_{cpl_aj_a}}. \tag{4}$$

$\tilde{\sigma}$ is the calculated DWBA cross section and the b's are the asymptotic normalization constants for the single particle bound state orbitals used in the DWBA. The sum in Eq. (3) is taken over the allowed orbital and total angular momentum couplings, and the C's are the ANC's for $a\rightarrow c+p$ and $A+p\rightarrow B$. For peripheral proton transfer, the above normalization of the DWBA cross section by the ANC's for the single particle orbitals makes the extraction of the ANC for $A+p\rightarrow B$ essentially independent of the parameters used in the single particle potential wells, in marked contrast to the more typical parametrization of the DWBA cross section in terms of spectroscopic factors. See Ref. [3] for additional details.

The angular distribution for the proton exchange reaction involving both the target and projectile ground states—elastic proton transfer—is shown in Fig. 4. DWBA calculations for the proton transfer were carried out with the finite-

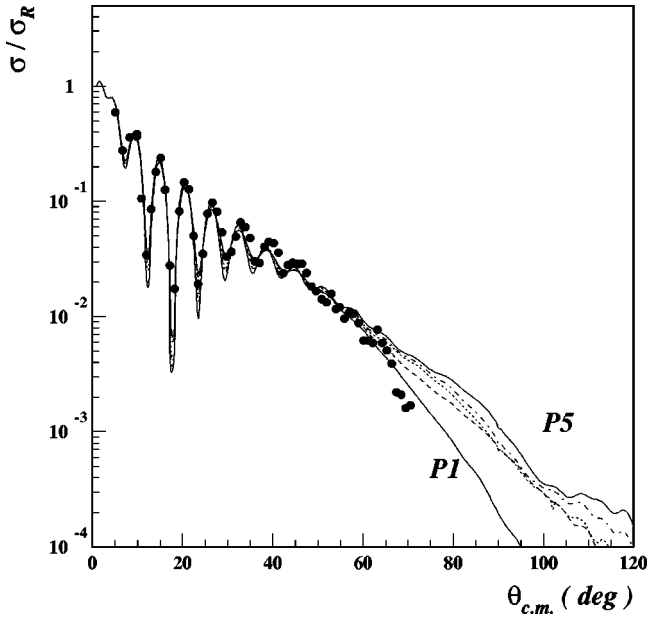

FIG. 3. The angular distribution for elastic scattering of 162 MeV ^{14}N on ^{13}C at forward angles. The curves are fits to the forward angle data using the optical model potentials P1 (solid), P2 (dashed), P3 (dotted), P4 (dash-dotted), and P5 (solid) of Table I.

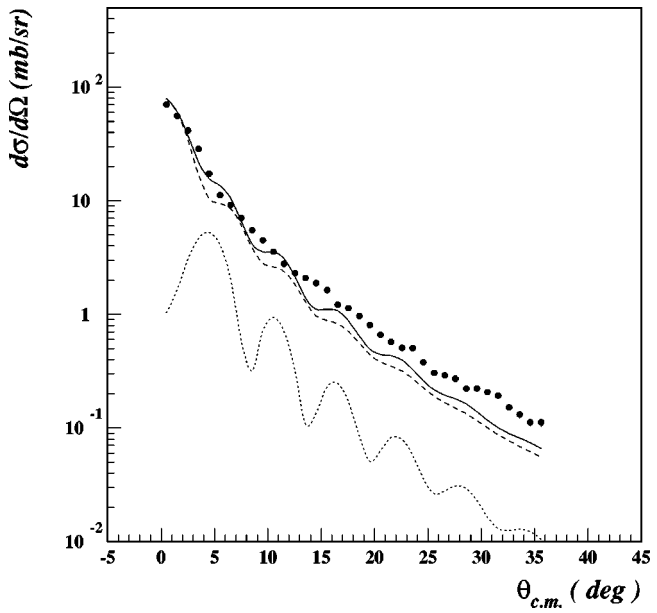

FIG. 4. The angular distribution measured for the elastic proton exchange reaction ^{13}C(^{14}N,^{13}C)^{14}N. The curves show the DWBA fit over the angular range $\theta_{\rm c.m.}=0-12°$ (full line), with $1p_{1/2}\rightarrow 1p_{1/2}$ (dashed line) and $1p_{1/2}\leftrightarrow 1p_{3/2}$ (dotted line) components.

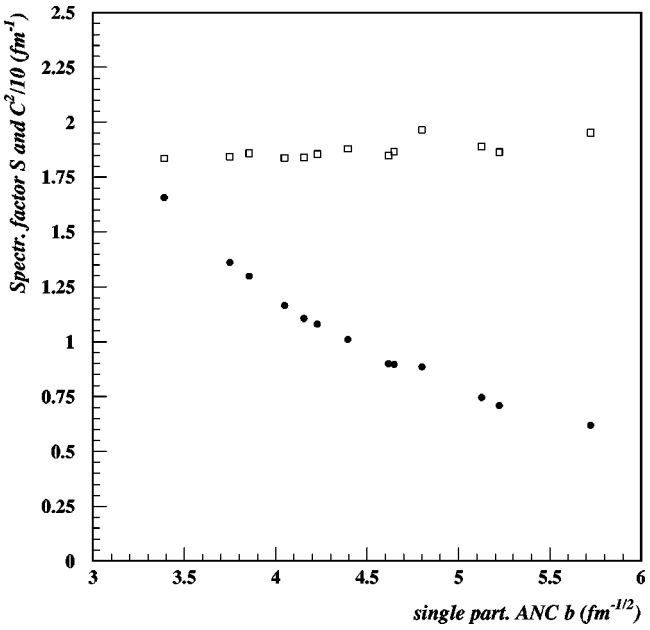

FIG. 5. The comparison between the spectroscopic factor $S_{p_{1/2}}$ (dots) and the ANC $C^2_{p_{1/2}}$ (squares) extracted for the ground state of ^{14}N as a function of the single particle ANC, $b_{p_{1/2}}$, used to normalize the DWBA calculations. Note that $C^2_{p_{1/2}}$ has been multiplied by 0.1.

range DWBA code PTOLEMY [11], using the full transition operator. Distorted waves were calculated using optical model potential P1 in Table I, and a standard Woods-Saxon well was used to bind the transferred proton to the remaining nuclear core. As was noted above, the spectroscopic factor associated with elastic transfer differs from the ANC by the normalization of the single particle wave function ANC's calculated in the same Woods-Saxon well. If a reaction is peripheral, this makes the extracted ANC quite stable over a broad range of single particle well parameters. In Fig. 5, we compare the ground state spectroscopic factor $S_{p_{1/2}}$ and ANC $C^2_{p_{1/2}}$ extracted for parameters of the single particle potential ranging from $r_0=1.0-1.3$ fm and $a=0.5-0.7$ fm, as functions of the value of the corresponding single particle ANC, $b_{p_{1/2}}$. It is clear from the figure that the spectroscopic factor depends strongly on the choice of the single particle potential parameters, while the ANC varies by less than 7% over the full range. If the choice of single particle well parameters is constrained to be within reasonable agreement with the measured rms charge radius [12], the variation of the ground state ANC $C^2_{p_{1/2}}$ is less than 3% whereas the spectroscopic factor varies by over 25%. A similar picture arises for $S_{p_{3/2}}$ and $C^2_{p_{3/2}}$, despite a substantially smaller contribution of the $1p_{3/2}$ orbital to the proton transfer cross section, and we take this as a confirmation of our fits for C^2_j. Another indication of the peripheral character of the reaction is the localization of the transfer strength with partial waves. For the elastic transfer, the DWBA transition matrix element is peaked around l values of 32, which corresponds semiclassically to $r=6.4$ fm, and has a full width at half maximum (FWHM) of about 10, making this reaction even more strongly focused on the surface than the ^{9}Be(^{10}B,^{9}Be)^{10}B elastic transfer reported in Ref. [3].

TABLE II. The asymptotic normalization coefficients for the $^{13}C+p\rightarrow{}^{14}N$ system, populating the ground and four excited states in ^{14}N. The calculations were done for the proton transferred from the ground state of the ^{14}N projectile to the ''final proton configuration'' in the specified ^{14}N states.

State in ^{14}N	J^π,T	Final proton configuration	$(C_{lj})^2$ [fm^{-1}]
g.s.	1^+,0	$1p_{1/2}$	18.6(12)
		$1p_{3/2}$	0.93(14)
2.313	0^+,1	$1p_{1/2}$	8.9(9)
3.948	1^+,0	$1p_{1/2}$	2.8(3)
5.106	2^-,0	$1d_{5/2}$	0.40(3)
5.834	3^-,0	$1d_{5/2}$	0.19(2)

From Eq. (3), the elastic proton transfer cross section is proportional to C^4 since the entrance and exit channels are identical. For the elastic transfer, we assumed a mixed configuration for the ground state of ^{14}N ($J^\pi=1^+,T=0$) in which the last proton in either the $1p_{1/2}$ or $1p_{3/2}$ orbital is coupled to the $1/2^-$ ground state of ^{13}C. Only the $1p_{1/2}\rightarrow 1p_{1/2}$ and $1p_{1/2}\leftrightarrow 1p_{3/2}$ contributions were considered since the admixture of the $1p_{3/2}$ orbital is small and the calculated angular distribution for $1p_{3/2}\rightarrow 1p_{3/2}$ is virtually indistinguishable from that for $1p_{1/2}\rightarrow 1p_{1/2}$. Note that the $1p_{1/2}\rightarrow 1p_{3/2}$ and $1p_{3/2}\rightarrow 1p_{1/2}$ contributions are identical due to time reversal invariance. Core excitations were not included since they should give a negligible contribution to the direct proton exchange. The DWBA calculation is compared to the data in Fig. 4. The solid line was found by combining contributions from the $1p_{1/2}$ and $1p_{3/2}$ components, weighted by the extracted C^2 for each j transfer. The extracted elastic transfer ANC's are given in Table II. The uncertainties in the extraction of the dominant $C^2_{p_{1/2}}$ term include the normalization of the cross section (3.5%), the choice of optical model parameters (3%), the stability of the fits as a function of the angular range considered (4%), and the choice of Woods-Saxon well parameters (1.5%). In particular, we found that the calculated DWBA transfer cross sections varied by only $\approx 2\%$ when going from one family of optical model parameters to the next, and therefore C^2 changed by only half that. This insensitivity of the ANC to the choice of optical model potential provides further support for the peripheral nature of the ^{13}C(^{14}N,^{13}C)^{14}N reaction at this energy because the elastic scattering was fitted in the angular range where it is essentially diffractive in nature and the potential at the surface is well determined.

In addition to the ground state, four of the excited states shown in Fig. 1 were populated with sufficient statistics to extract ANC's. The one exception is the ^{13}C excited state at 3.089 MeV. We assume this state was populated by removing a $2s_{1/2}$ proton from the small $2s^2_{1/2}$ component of the ^{14}N ground state. At small angles where the ^{13}C excited state was clearly visible, the observed angular distribution is consistent with a 2–3 % admixture of this configuration in the ^{14}N ground state.

The angular distributions for transitions to the ^{14}N excited states at 2.313, 3.948, 5.106, and 5.834 MeV are shown in Fig. 6, together with their calculated DWBA fits. In each case, the calculation was carried out by considering the tran-

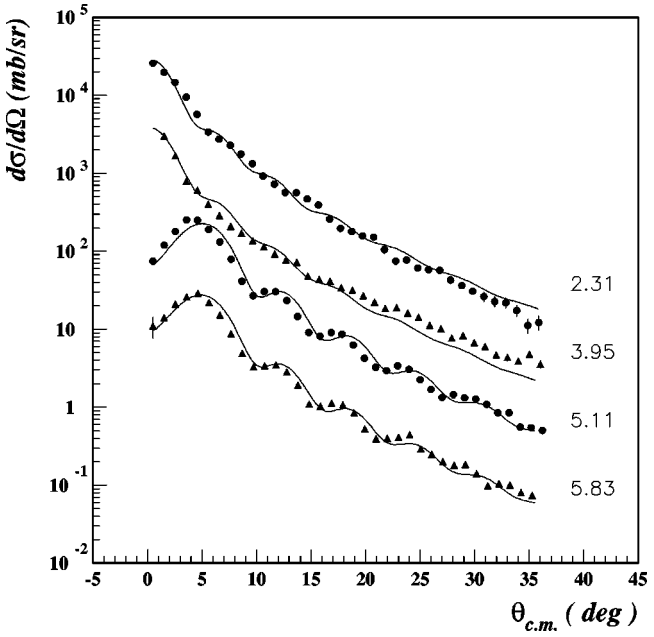

FIG. 6. The angular distributions for inelastic proton transfer to the ^{14}N excited states at 2.313, 3.948, 5.106, and 5.834 MeV, multiplied by factors of 10^3, 10^2, 10, and 1, respectively. The curves show the corresponding DWBA fits, as described in the text.

sition from the ^{14}N ground state to the final proton configuration shown in Table II and yielded the ANC specified. For the first excited state in ^{14}N, the DWBA fit shown in Fig. 6 includes $1p_{1/2}\rightarrow 1p_{1/2}$ and $1p_{3/2}\rightarrow 1p_{1/2}$ proton transfer terms, weighted by the $C^2_{p_{1/2}}$ and $C^2_{p_{3/2}}$ ANC's found above for the ^{14}N ground state, respectively. A separate fit which allowed these two terms to vary independently gave a result for $C^2_{p_{3/2}}/C^2_{p_{1/2}}$ for the ground state that was consistent with the value found above, but with reduced precision. For the second excited state, we considered contributions from $1p_{1/2}\rightarrow 1p_{1/2}$, $1p_{1/2}\rightarrow 1p_{3/2}$, and $1p_{3/2}\rightarrow 1p_{1/2}$ proton transfers. The latter two gave similar calculated angular distributions and were combined. We found the $1p_{1/2}\leftrightarrow 1p_{3/2}$ contribution to be very much smaller than the $1p_{1/2}\rightarrow 1p_{1/2}$ term given in Table II. The ^{14}N third and fifth excited states, which form the $(1p_{1/2}\cdot 2s_{1/2})_{0^-,1^-}$ doublet, were only weakly populated due to the angular momentum mismatch and could not be resolved from the fourth and sixth excited states, respectively. The ^{14}N fourth and sixth excited states are members of the $(1p_{1/2}\cdot 1d_{5/2})_{2^-,3^-}$ doublet, and their characteristic oscillations are well described by the calculated $1p_{1/2}\rightarrow 1d_{5/2}$ angular distribution. However, a 0.7° shift is observed between the measured and calculated oscillations. Attempts to include $1p_{3/2}\rightarrow 1d_{5/2}$ or $1p_{1/2}\rightarrow 2s_{1/2}$ terms, the latter to account for the weak unresolved states, did not improve the fits. A similar situation, but with a shift of 2°, was seen in a previous ^{13}C(^{7}Li,^{6}He)^{14}N proton transfer experiment [13]. As was noted above for the elastic transfer, the ANC's extracted for transfer to the excited states depend only weakly on the assumed bound state parameters or the choice of optical model potential. The uncertainties quoted in Table II for the excited state ANC's are determined primarily by the uncertainty in the normalization of the cross section (3.5%) and the added uncertainties due to the choice of optical model potential parameters (3%) and the quality and stability of the fits (4% or larger). It is worth noting that the normalization and optical potential uncertainties are correlated for all of the ANC's in Table II.

V. CONCLUSIONS

We have measured the elastic scattering ^{13}C(^{14}N,^{14}N)^{13}C and the elastic and inelastic proton exchange reaction ^{13}C(^{14}N,^{13}C)^{14}N leading to the ground state and four excited states in ^{14}N. The measurements of the proton transfer reaction have been used to extract the ANC's describing the tail of the wave function of the outer proton in ^{14}N in the field of the ^{13}C core. The ANC's found here will be used to extract the ANC for ^{7}Be$+p\rightarrow$ ^{8}B from the proton transfer reaction ^{14}N(^{7}Be,^{8}B)^{13}C.

ACKNOWLEDGMENTS

This work was supported in part by the U.S. Department of Energy under Grant No. DE-FG05-93ER40773 and by the Robert A. Welch Foundation.

[1] A. M. Mukhamedzhanov and N. K. Timofeyuk, JETP Lett. **51**, 282 (1990).
[2] H. M. Xu, C. A. Gagliardi, R. E. Tribble, A. M. Mukhamedzhanov, and N. K. Timofeyuk, Phys. Rev. Lett. **73**, 2027 (1994).
[3] A. M. Mukhamedzhanov, H. L. Clark, C. A. Gagliardi, Y.-W. Lui, L. Trache, R. E. Tribble, H. M. Xu, X. G. Zhou, V. Burjan, J. Cejpek, V. Kroha, and F. Carstoiu, Phys. Rev. C **56**, 1302 (1997).
[4] D. M. Pringle, W. N. Catford, J. S. Winfield, D. G. Lewis, N. A. Jelley, K. W. Allen, and J. H. Coupland, Nucl. Instrum. Methods Phys. Res. A **245**, 230 (1986).
[5] D. H. Youngblood and J. B. Bronson, Nucl. Instrum. Methods Phys. Res. A **361**, 37 (1995).
[6] D. H. Youngblood, Y.-W. Lui, H. L. Clark, P. Oliver, G. Simler, and Nucl. Instrum. Methods Phys. Res. A **361**, 359 (1995).
[7] S. Kowalski and H. A. Enge, computer code RAYTRACE, 1986 (unpublished).
[8] F. Ajzenberg-Selove, Nucl. Phys. **A523**, 1 (1991).
[9] F. Carstoiu, computer code OPTIMIX (unpublished).
[10] D. E. DiGregorio, J. Gomez del Campo;, Y. D. Chan, J. L. C. Ford, Jr., D. Shapira, and M. E. Ortiz, Phys. Rev. C **26**, 1490 (1982).
[11] M. Rhoades-Brown, M. McFarlane, and S. Pieper, Phys. Rev. C **21**, 2417 (1980); **21**, 2436 (1980).
[12] H. de Vries, C. W. de Jager, and C. de Vries, At. Data Nucl. Data Tables **36**, 495 (1987).
[13] J. Cook, M. N. Stephens, and K. W. Kemper, Nucl. Phys. **A466**, 168 (1987).